



Experimental and CFD Study of a Sub-scale Rotating Detonation Combustor Fed with Gaseous H_2-O_2

Ewen BARD ¹, Dmitry DAVIDENKO ¹, Wolfgang ARMBRUSTER ², Stéphane BOULAL ¹, Michael BÖRNER ², Justin S. HARDI ² Pierre VIDAL ³

Abstract

Understanding the physical phenomena in a Rotating Detonation Engine combustor is essential for its practical application. Sub-scale Rotating Detonation Combustor testing enables extensive investigation under diverse conditions, clarifying the factors that influence detonation characteristics. Numerical simulations further enhance the comprehension of the combustor dynamics by revealing the intricate interactions from mixture formation to detonation, with a consensus highlighting mixture formation as key to stable, efficient detonation. A collaboration between ONERA and DLR is studying a subscale RDE combustor fed with gaseous H_2/O_2 . DLR manufactured and tested the combustor at the Lampoldshausen Centre, yielding data on injection parameters and detonation characteristics (wave number, propagation direction, and velocity). ONERA employs its CFD code CEDRE in an LES approach, modeling the entire chamber with the injector to capture the unsteady effects of periodic detonations on injection and mixing. This article presents experimental and numerical results for some selected cases, illustrating the alignment between both methods and offering insights into the mechanisms driving specific detonation regimes, particularly focusing on fresh mixture formation and conditions in the refill region.

Keywords: rotating detonation, injection, detonation regime, co-rotating, counter-rotating

Nomenclature

Latin

D − Measured wave velocity

L − Chamber length

 N_w - Number of waves ROF - Oxidizer to fuel ratio or mixture ratio

1. Introduction

In the 1960s, Voitsekhovskii introduced the concept of a Rotating Detonation Combustor (RDC), in which one or more detonations can propagate continuously consuming fresh propellants injected between successive detonation waves. Theoretically, using detonation instead of deflagration increases engine efficiency compared to conventional engines, as demonstrated by Wolański [27]. Despite promising results from the studies by Naples et al. [21], Frolov et al. [14], and Bach et al. [2], no experimental research has concretely shown an efficiency gain from RDCs, to the best of the authors' knowledge.

Empirical laws related to RDC geometry, as proposed by Bykovskii et al. [10], and the reduced model by Kaemming et al. [17] can help identify key parameters for ensuring stable operation, high thrust efficiency, and pressure gain in an RDC. However, they do not account for the mixing characteristics of fresh propellants in the chamber, a crucial factor for RDC efficiency, as highlighted by Sun et al. [26]. Conversely, complex 3D simulations of entire RDCs have been conducted by various authors, e.g.,

¹ONERA, Université Paris-Saclay, DMPE, 6 Chemin de la Vauve aux Granges, Palaiseau, 91123, France, ewen.bard@onera.fr / dmitry.davidenko@onera.fr

²Institute of Space Propulsion, DLR - German Aerospace Center, Im Langen Grund, Hardthausen am Kocher, 74239, Germany, wolfgang.armbruster@dlr.de

³Institut Pprime CNRS UPR 3346, 11 Boulevard Marie et Pierre Curie Site du futuroscope, Futuroscope-Chasseneuil, 86961, France, pierre.vidal@ensma.fr

Cocks et al. [11], Liu et al. [20], Pal et al. [23], Prakash et al. [24], and Nassini [22] to study detonation propagation conditions and confirm engine efficiency. Yet, these simulations are too computationally expensive for practical use in the design process. Hellard et al. [16] used a simplified numerical simulation approach to study propellant mixing by focusing on the injection of the RDC. This method significantly reduced computational costs while retaining essential physics, and helped to refine the design, especially around the injectors.

This study relates to stable detonation regimes observed experimentally. 3D reactive LES computations with the corresponding boundary conditions are conducted to study the main phenomena governing the fresh mixture formation and its consumption by the detonation front. This study focuses more particularly on the numerical reproductions of two regimes observed experimentally: a 3-wave co-rotating and a 5-wave counter-rotating regime under their respective geometrical, mass flow rate, and mixture ratio (ROF) conditions. Both regimes are compared to one another to highlight the benefits of co-rotating fronts over counter-rotating fronts. First, the experimental cases are introduced by describing the chamber geometry, test conditions, and essential results. Second, the numerical study is presented through the CFD approach and results for the chosen cases. Finally, a brief discussion concludes the paper.

2. Experimental setup and results

The experimental RDC was tested with H_2/O_2 on two different test facilities at the DLR centre of Lampoldshausen, achieving low (16 to 75 g/s) and high mass flow rates (50 to 300 g/s) ([1, 3, 4]). The outer diameter of the RDC is 68 mm. Figure 1 shows (a) the implementation at the test facility for low mass flow rate tests, and (b) a section cut of the two tested configurations. The low flow rate case corresponds to the chamber configuration with a 60 mm long duct and an annular gap of 4.5 mm. For the high flow rate case, the chamber length is 42 mm and the annular gap is 10 mm. These differences are due to the centre body diameter and length.

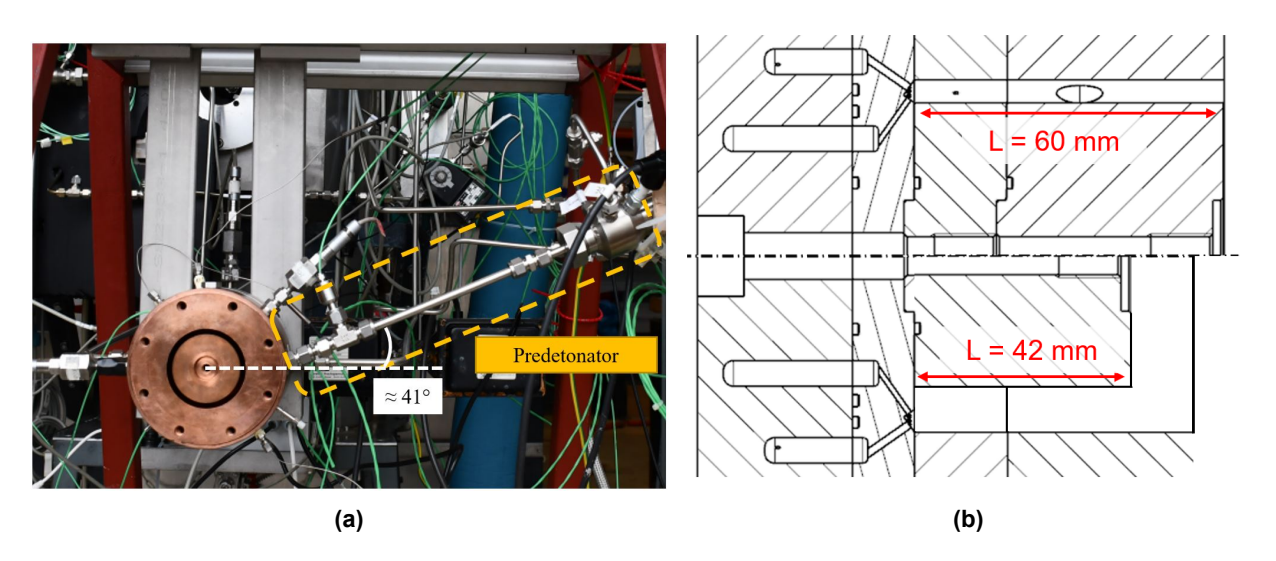


Fig 1. RDC installation on a test bench (a). Cross-sectional cut of the experimental RDC (b): narrow annular gap of 4.5 mm (top) and wide gap of 10 mm (bottom)

The injector has 72 injection elements, one every 5° angle. Figure 2 shows the geometry of an injection element. It consists of an unlike doublet of perpendicular impinging jets. The diameters of the injection orifices for H_2 and O_2 are, respectively, 1 and 1.5 mm.

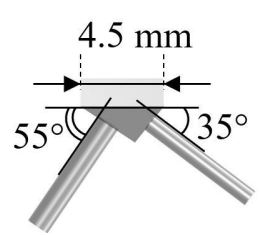


Fig 2. Injector element geometry
The observed detonation regime for the high flow rate case is characterised by 3 co-rotating fronts. For the low flow rate case, there are 5 counter-rotating fronts (5 fronts in each direction). Table 1 shows the experimental conditions for both regimes.

Table 1. Experimental conditions for 3-wave co-rotating and 5-wave counter-rotating
regimes

Simulation Case	Total mass flow rate (g/s)	ROF	O ₂ mass flow rate (g/s)	O ₂ Plenum pressure (bar)	H ₂ mass flow rate (g/s)	H ₂ Plenum pressure (bar)
3-wave co-rotating	203	6.4	175.7	7.5	27.3	10
5-wave counter-rotating	37.2	7.9	33	1.8	4.2	1.9

The back-end of the RDC was visualized by means of a high-speed camera at a frame rate of 180 kHz. During the image post-processing [5, 6], a diagram representing the average pixel intensity over the annulus width is unwrapped over the circumference and plotted against the time to track the wave-front dynamics. Figure 3 shows the azimuthal angle-time diagram of the 3-wave co-rotating regime obtained with the high flow rate. The diagram shows equidistant tracks of detonation waves with almost constant luminosity and inclination, which prove stable operation. Considering the front frequency and the outer diameter of the chamber, the mean propagation velocity is 2410 m/s. The purple band at $\sim 90^{\circ}$ angle in the lower part of the diagram corresponds to high-speed camera saturation due to burning of the pressure sensor coating during the test.

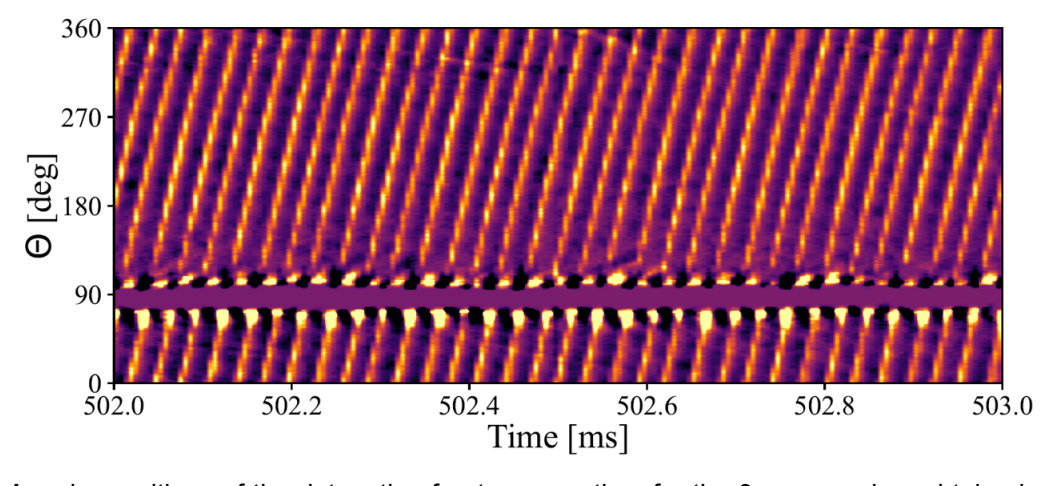


Fig 3. Angular positions of the detonation fronts versus time for the 3-wave regime obtained with the high flow rate

Figure 4 shows the angle-time diagram for the 5-wave counter-rotating regime obtained with the low flow rate. Such kind of regime was often observed in other tests at the same test facility. The white lines help the reader to recognize some of the wave tracks. The green and blue lines highlight the path of two different fronts colliding at an angular position of 180°. The diagram shows a regular pattern with almost constant angular positions of the track intersections, which means that each group of 5 fronts propagates at the same speed and the waves in each group are uniformly spaced.

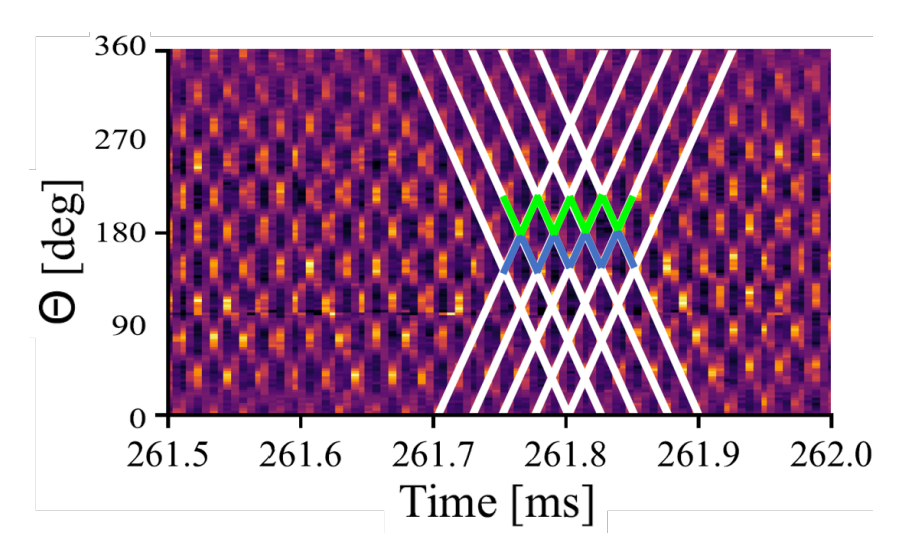


Fig 4. Angular positions of the detonation fronts versus time for the 5-wave counter-rotating mode obtained with the low flow rate

3. Simulation approach

3.1. Numerical method

For this study, Large Eddy Simulations (LES) are performed with the CEDRE code, the multiphysics software developed at the DMPE (Multi-Physics for Energetics Department) of ONERA ([25]). CHARME (also described in [25]) is the solver for the Navier-Stokes equations for a compressible reactive flow. The finite volume method is employed for spatial discretization on general unstructured meshes. The convective fluxes are calculated by means of the MUSCL (Monotonic Upstream Scheme for Conservation Laws) [19] interpolation scheme, in combination with the Van Leer slope limiter, which provides a second-order accuracy. The viscous fluxes are computed with a central difference second-order scheme. A first-order implicit Euler scheme and a timestep of 10^{-9} s are used for time integration. The Smagorinsky model is chosen to account for the effect of subgrid turbulence scales. Chemical reactions of the H_2/O_2 system are modeled with a 7-species and 7-reaction kinetic mechanism proposed by [12]. It has been validated for H_2/O_2 detonation cases ([13, 15]).

3.2. Computational domain and boundary conditions

For 3D LES, the computational domain can be restricted to the high flow rate of the full combustor with an angular span of $360^{\circ}/N_{w}$, where N_{w} is the number of wave fronts propagating in the same direction. By applying periodic boundary conditions at the radial planes delimiting the domain, it is possible to simulate established wave propagation of only one detonation wave front (or two in the case of counter-rotating modes) per sector, significantly reducing the computational cost. In this study of 3- and 5-wave regimes, the domain is limited to $1/3^{rd}$ and $1/5^{th}$ of the full combustor. Figure 5 shows the two computational domains considered in this study.

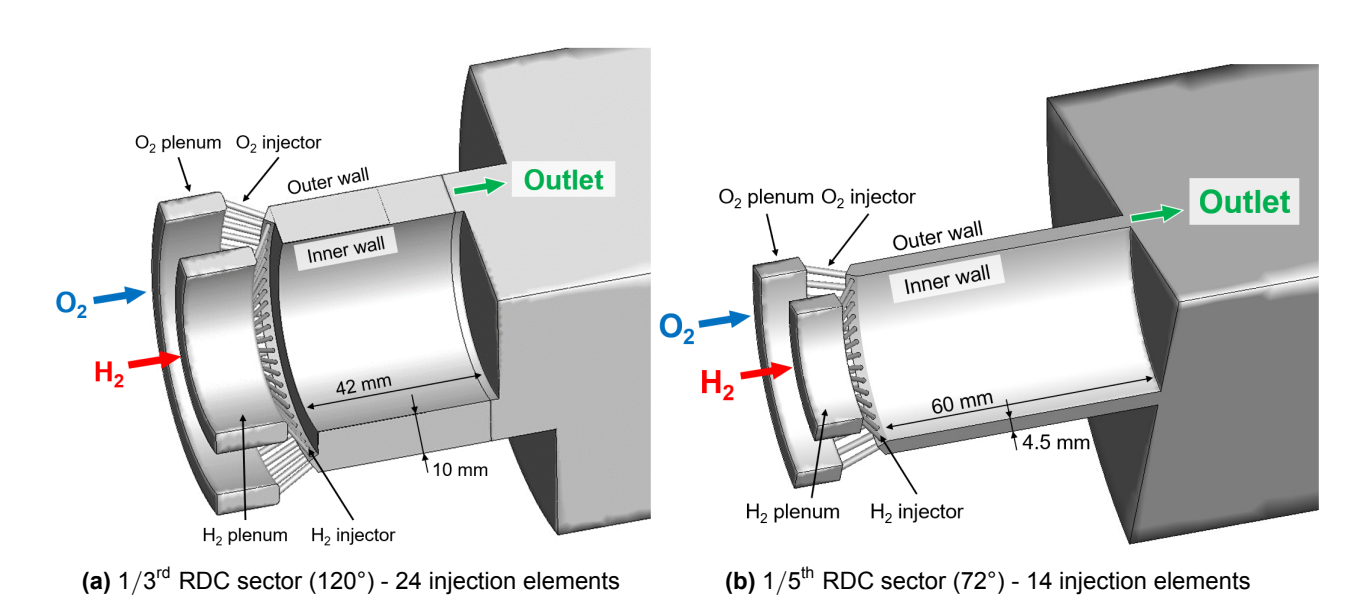


Fig 5. 3D domains for simulations of the 3-wave (a) and 5-wave (b) regimes

For the 3-wave regime, the mesh is composed of approximately 9 million tetrahedra, with a minimum cell size of 180 μ m in the area where the propellant jets impinge. The mesh of the 5-wave counter-rotating regime is composed of approximately 15 million tetrahedra, with a minimum cell size of 100 μ m in the area near the impingement of the propellant jets. For both cases, the mesh size is gradually increased along the chamber length away from the mixing zone.

The boundary conditions (see Fig. 5) are as follows. A non-slip condition is applied to the wall surfaces. Adiabatic conditions are imposed on the walls of the propellant plenums and the injector tubes. The chamber walls are at a fixed temperature of 400 K. A periodic boundary condition in the azimuthal direction is applied to the radial boundaries. The mass fluxes conformal to the experimental propellant flow rates are imposed at the inlet of each plenum.

A total temperature of 293 K is specified for both propellants. Both domains have a large damp volume at the chamber exit to evacuate the combustion products and the shocks emanating from the chamber. Constant atmospheric pressure and non-reflecting conditions are imposed over the outflow boundary of the damp volume.

3.3. Initial condition

The flow field is first initialized with a non-reactive cold flow in the plenum and injector subdomains, using atmospheric pressure conditions at the injector outlet. The chamber domain is initialized with a flow field from a 2D simulation with a simplified configuration and premixed injection, and wrapped along the chamber mid-circumference. This solution is then extended radially to cover the radial gap. Figure 6 shows the temperature field over a slice at the injector mid radius with the projected 2D solution. The blue area represents the homogeneous fresh mixture layer.

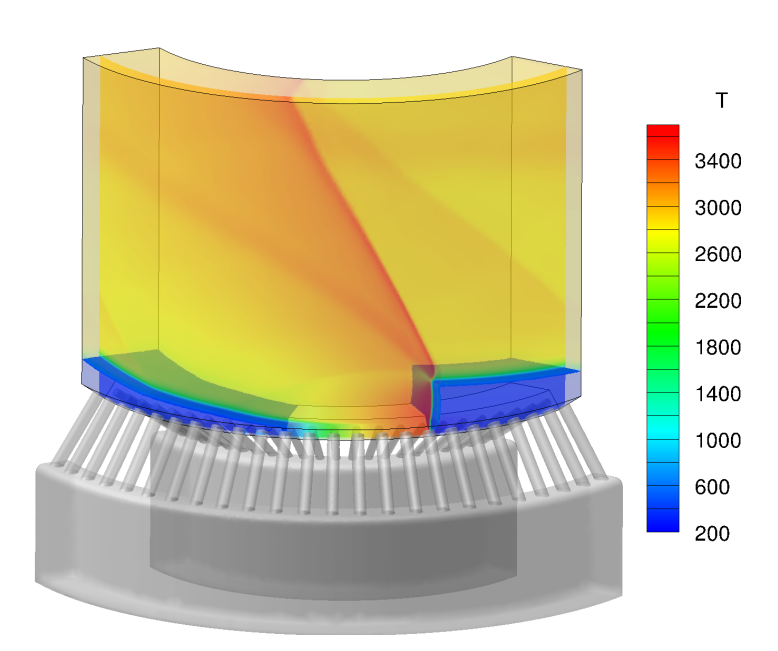


Fig 6. Flow field initialization with a 2D solution: temperature field.

4. Simulation results

4.1. Three-wave Co-rotating regime

Figure 7 shows the instantaneous and phase-averaged temperature fields at the injector mid-radius (31.75 mm) unwrapped on the x-theta, where x is the distance from the chamber bottom and theta is the azimuthal angle plane. The averaging process is described later in this section. Turbulent motions strongly perturb the instantaneous flow field. Its structure is clearer in the averaged field. The blue zone corresponds to the fresh mixture layer. The step of its triangular shape corresponds to the detonation front. The developed turbulent structures at the upper edge of the mixture layer cause intense deflagration of the fresh mixture in contact with the burnt gases. Unburnt gas pockets are visible behind the detonation front, indicating that some propellant mass remains unmixed.

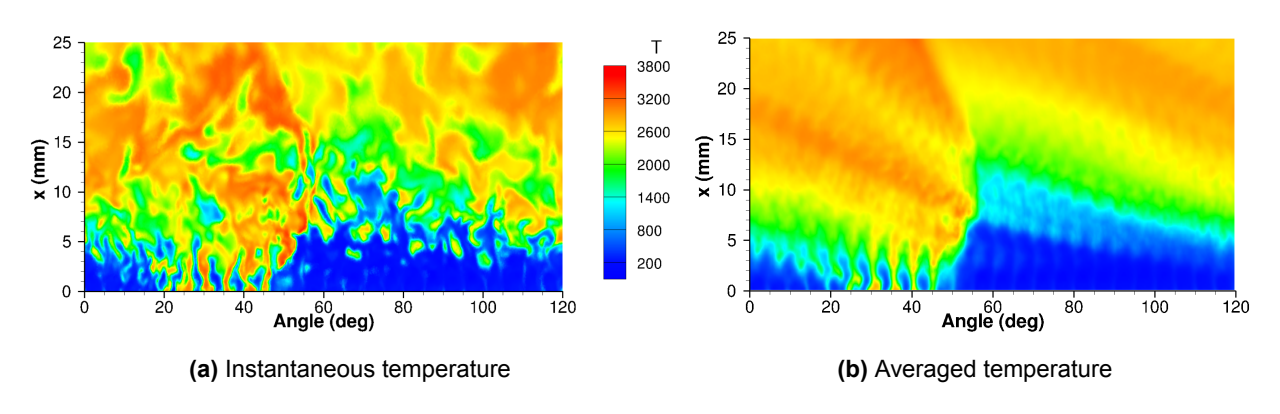


Fig 7. Temperature fields at the injector mid-radius for the 3-wave co-rotating regime

The detonation velocity is determined by analyzing pressure signals recorded by several numerical sensors located on the outer wall. Figure 8 shows the evolution of the detonation velocity D over more than 9 cycles of propagation corresponding to 3 full combustor revolutions. The mean value of the front velocity over this period is 2576 m/s. For comparison, the experimentally observed detonation velocity in the same regime is 2410 m/s. This means the simulation overestimates the detonation velocity by

about 160 m/s. Several factors could be responsible for this difference, among which are the simplified reaction kinetics, the basic subgrid turbulence model, and insufficient mesh resolution. Moreover, the heat release and wall interactions cannot be resolved precisely due to the coarse mesh resolution and artificial boundary conditions at the wall.

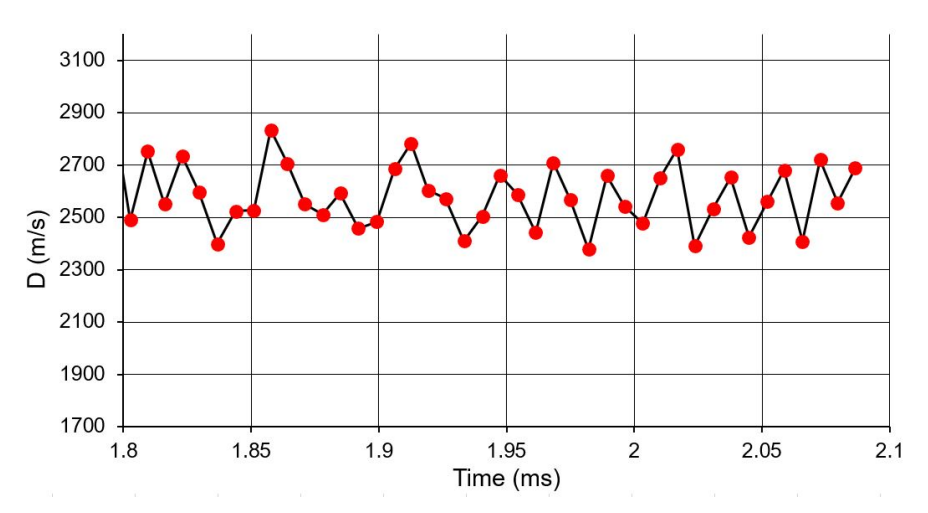


Fig 8. Detonation wave velocity at the outer radius of the combustor

Analysis of the fresh mixture state consumed by the detonation requires averaging of a large number of instantaneous flow fields. These flow fields are collected during 3 detonation propagation periods. To obtain a phase-averaged field, a frame attached to the detonation wave was used. The detonation front, defined in a first approach as the isobaric surface at 5 bar, is shifted to the central injection element of our considered sector. By doing this procedure for 73 instantaneous flow fields, the detonation front is always kept near the same element. The zone ahead of the front is considered for the following analysis. Figure 9 shows the zones defined for the analysis of the phase-averaged flow field. Three of these zones are placed over the injector elements 12 to 14, from left to right. As for the two additional zones, their positions are shifted by half of the element angular span. The zones are 25 mm high and radially spread over the 10 mm annular gap of the combustor. Their azimuthal span is 5°, which corresponds to a single injection element.

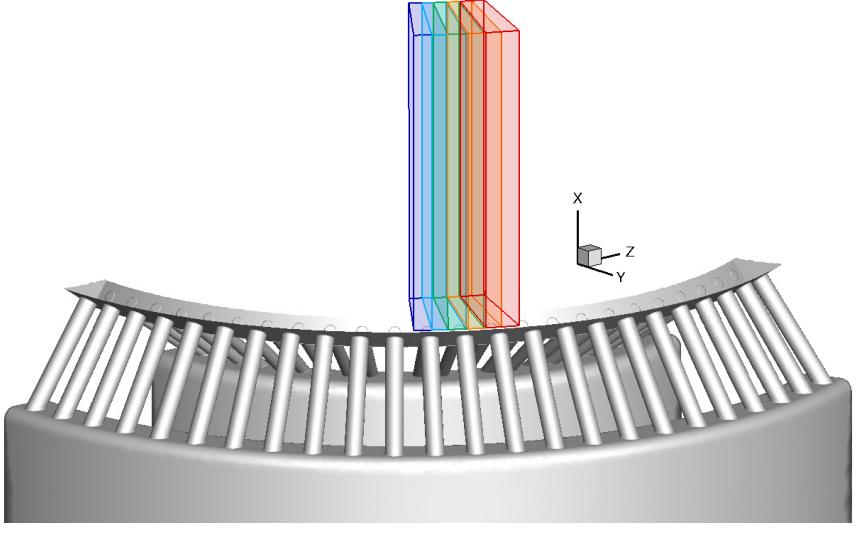


Fig 9. Five zones for averaged flow field analysis

The gas properties in each volume are processed by averaging them in planes normal to the chamber axis. The obtained profiles along the x-axis are presented in the following figures. Figure 10 shows profiles of the equivalence ratio and fluid mass integral along the x-axis for the chosen control volumes. The volumes number 12 and 12-13 are within the zone perturbed by the detonation, so the corresponding profiles are not aligned with the other ones. The three remaining profiles are fairly aligned, so the choice of the control volume position within the corresponding range is not important for the analysis. The equivalence ratio is near the nominal level (\sim 1) within a distance of 0 to 5 mm. Then its value quickly increases, but this can result from fresh mixture consumption by deflagration. The mass integral shows a slope break at 6 mm because the above zone is mainly filled with burnt gases.

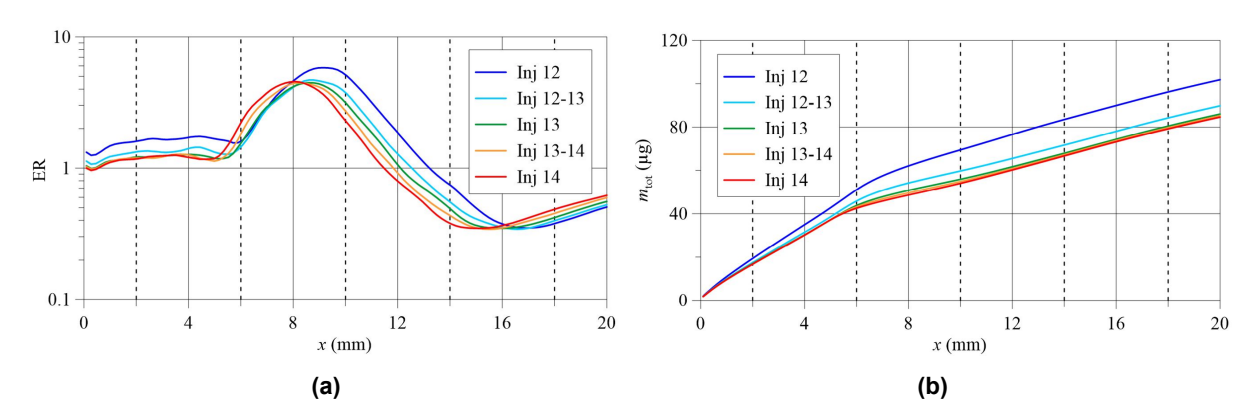
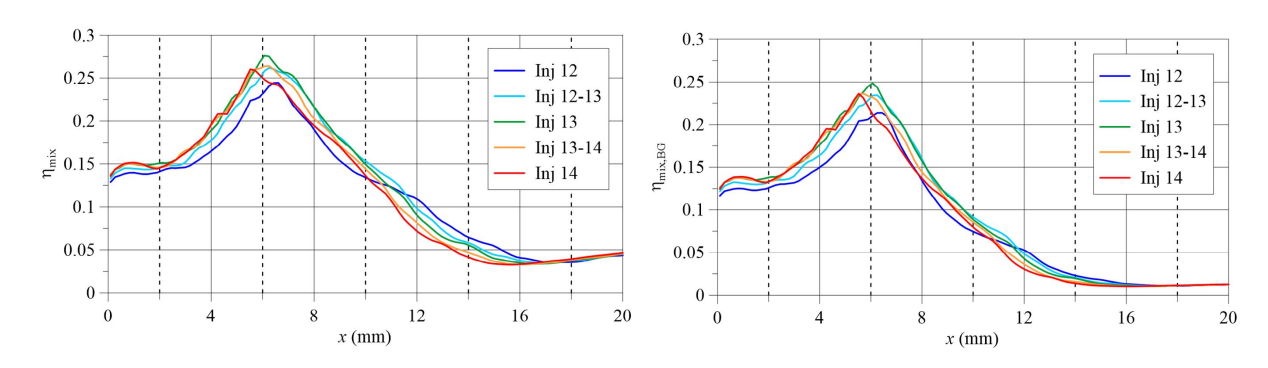


Fig 10. Profiles of equivalence ratio and fluid mass integral versus distance from the chamber bottom for the chosen control volumes

The mixing efficiency, defined by equation 1 [18],

$$\eta_{\mathsf{mix}}(x) = \frac{\iint_{S_y} \frac{\rho Y_{H_2}}{\max(ER, ER_{glob})} \, dy \, dz}{\iint_{S_y} \frac{\rho Y_{H_2}}{\min(ER, ER_{\mathsf{glob}})} \, dy \, dz} \tag{1}$$

corresponds to the mass fraction of fresh gases that are in proportions that respect the global equivalence ratio of the chosen operating point (ERglob). ER is the local equivalence ratio. Figure 11 shows the evolution of the mixing efficiency, considering only the fresh propellants (Fig. 11a) and taking into account the fraction of the burnt gas (Fig. 11b).



(a) Mixing efficiency without burnt gases considered
(b) Mixing efficiency with burnt gases considered
Fig 11. Profiles of mixing efficiency versus distance from the chamber bottom for the chosen control

volumes

The maximum efficiency in both cases is achieved at \sim 6 mm downstream of the injection plane. Additionally, the consideration of the mass fraction of burnt gases slightly reduces the mixing efficiency

within this distance.

Figure 12 shows the evolution of the burnt gases mass fraction and the heat release rate along the x-axis. It clearly appears that the profiles for volumes 12 and 12-13 show distinguishably higher maxima of heat release at $x = \infty 8$ mm when compared to the other volumes. This is a direct sign that the detonation front, and more specifically, the reaction zone, affects those first two volumes. This interpretation can also be derived from Fig. 12a, where volumes 12 and 12-13 contain higher proportions of burnt gases in the region close to the injector ($x \le 5$ mm). The other profiles indicate that burnt gases account for nearly 15% of the mixture mass in this region.

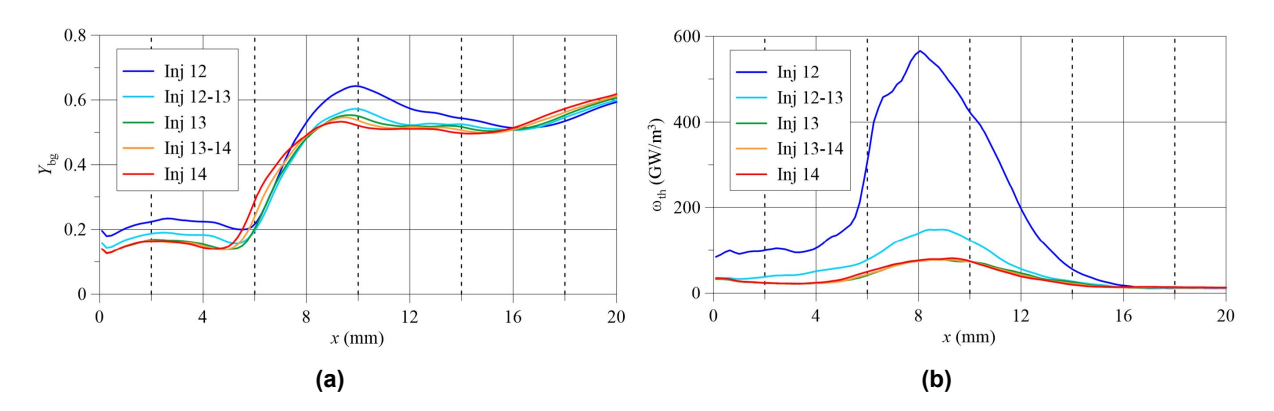


Fig 12. Profiles of mass fraction of burnt gas and heat release rate versus distance from the chamber bottom for the chosen control volumes

Finally, using equation 2,

$$\eta_{\text{def}} = 1 - \frac{m_{fg}}{m_{ini}} \tag{2}$$

where m_{fg} is the integral mass of burnt gas and m_{inj} is the total injected mass during one detonation cycle through a single injection element, the fraction of the injected propellant mass burnt in deflagration mode is about $32 \pm 1\%$ for volumes 13, 13-14 and 14, which are considered to be representative of the fresh mixture consumed by detonation.

4.2. Five-wave counter-rotating regime

The operating modes obtained at lower mass flow rates were primarily characterized by counter-rotating detonation waves. These waves travel in opposite azimuthal directions and repeatedly collide with one another. Such an operation represents a marginal regime for RDEs, and hence is to be mitigated. Their propagation velocity tends to be variable between the collisions, as the refilling of propellant at the collision points of the shock waves is less efficient than in co-rotating detonation regimes. Experimental studies, including those by Bluemner et al. [7], consistently report a greater velocity deficit relative to the Chapman-Jouguet (CJ) velocity $D_{\rm CJ}$ compared to co-rotating regimes with an equivalent number of detonation fronts, but without the opposing wave interactions. Figure 13 shows the instantaneous temperature field in a slice at the mid radius of the combustor, when two waves move away right after their collision.

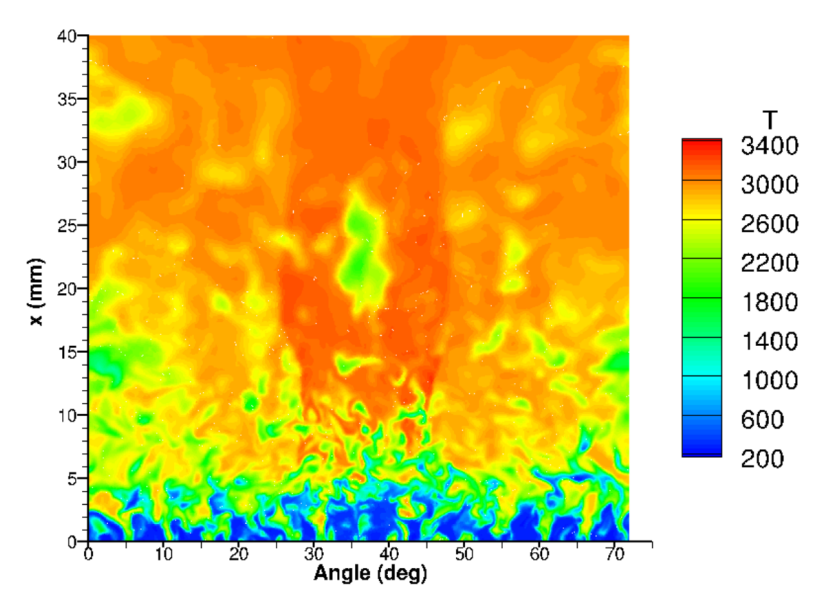


Fig 13. Instantaneous temperature field after collision event of two wave fronts

Similar to the previous post-processing method, the propagation of the wave fronts was studied after averaging 30 different instantaneous states over 14 injection elements. Figure 14 shows the highlighted volume layer between 1 and 3 mm downstream of the injector, where the maximum pressure and heat release are observed. The field is colored with the pressure values and shows a pressure rise in the middle of the sector as a consequence of the previous collision event between two wave fronts.

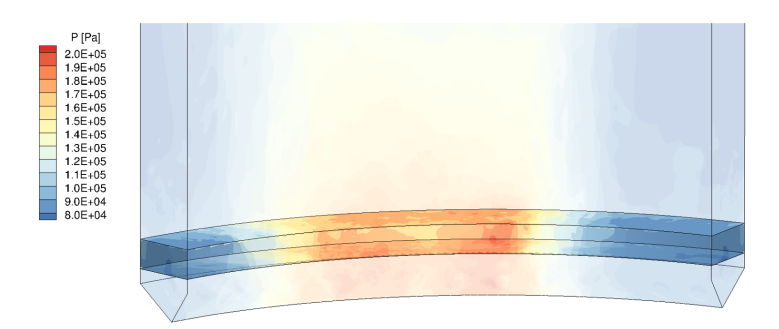


Fig 14. Volume layer for results averaging for the 5-waves counter-rotating case

Figure 15 shows a 3D diagram of the evolution of pressure (top) and heat release (bottom) as a function of time and the injector position. The cycle starts on the left side right after the collision of two wave fronts (first yellow curve). Evolving from 2 to \sim 13 µs towards the right side of the diagram, the wave fronts first spread apart from each other towards the background and foreground sides of the diagram (injectors 1 and 14), thus showing a decrease in pressure, even reaching a quasi balanced state over all injectors (around 8 µs, blue curve). The next collision occurs then between 12 and 16 µs (red and brown curves). Then the wave fronts move towards the center of the sector before the next collision happens on the right side of the diagrams (at \sim 26 µs, and centered on injectors 7 to 8).

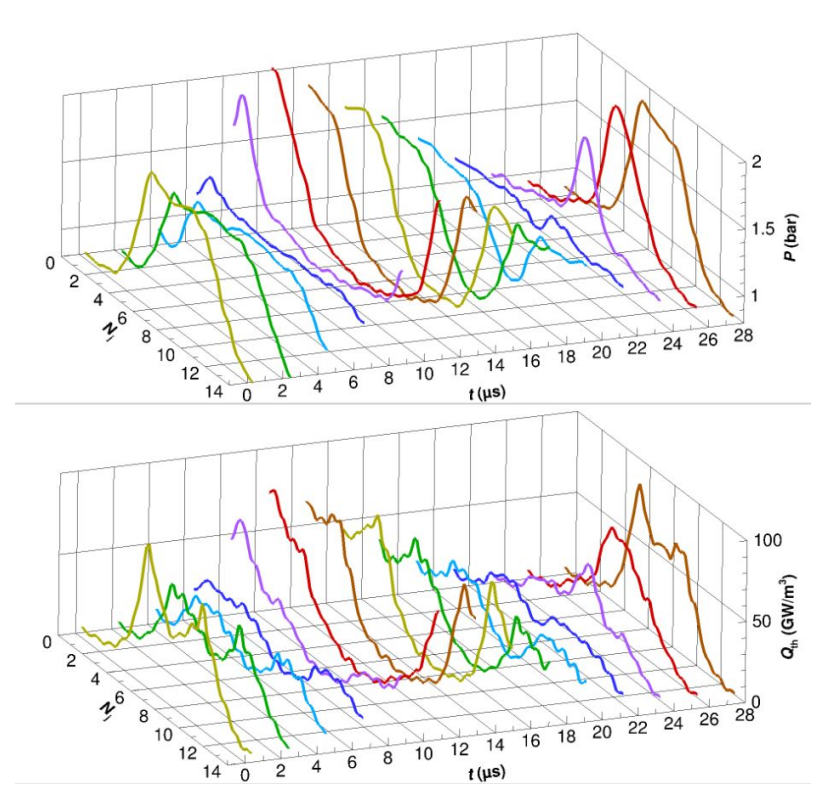


Fig 15. Pressure and heat release evolution as a function of the injector element position and over time

Figure 16 shows the evolution of the maximum chamber pressure and integral heat release rate, during a complete cycle (Fig. 15). This evolution confirms the overall propagation pattern, with wave collisions at the beginning, in the middle (\sim 12 μs), and at the end of the cycle. One can observe a small shift between the curves, always featuring the rise in pressure (blue curve) followed by the heat release (red curve). This might be the sign of a decoupling between the shock waves and the chemical reaction zone after the collision event.

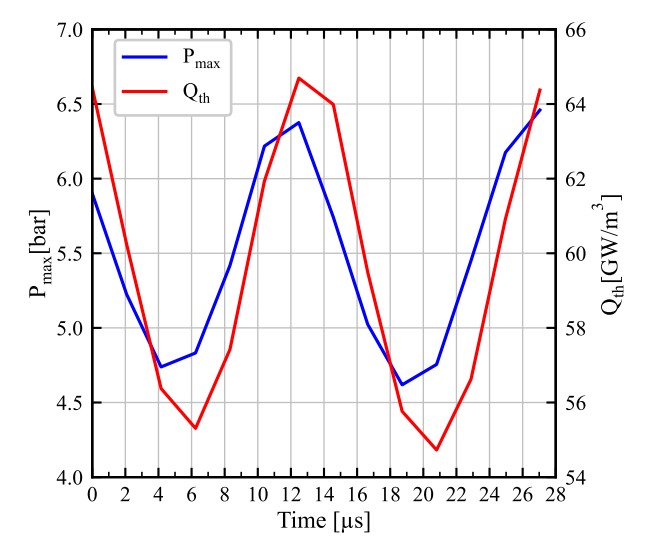


Fig 16. Evolution over one cycle of the maximum pressure and integral heat release rate

4.3. General discussion

Figure 17 compares the time average pressures recorded by numerical sensors placed against the injection elements for the 5-wave counter-rotating regime and the pressures averaged in time and space for the 3-wave co-rotating regime. Indeed, in the last case, the detonation pattern remains constant in both space and time. Also, the mean pressure is divided by the minimum value found between successive peaks to compensate for the difference in the mass flow rate between the two cases. The counter-rotating regime shows periodic variations. The values obtained for the 3-wave co-rotating regime are approximately double the values of the 5-wave counter-rotating regime.

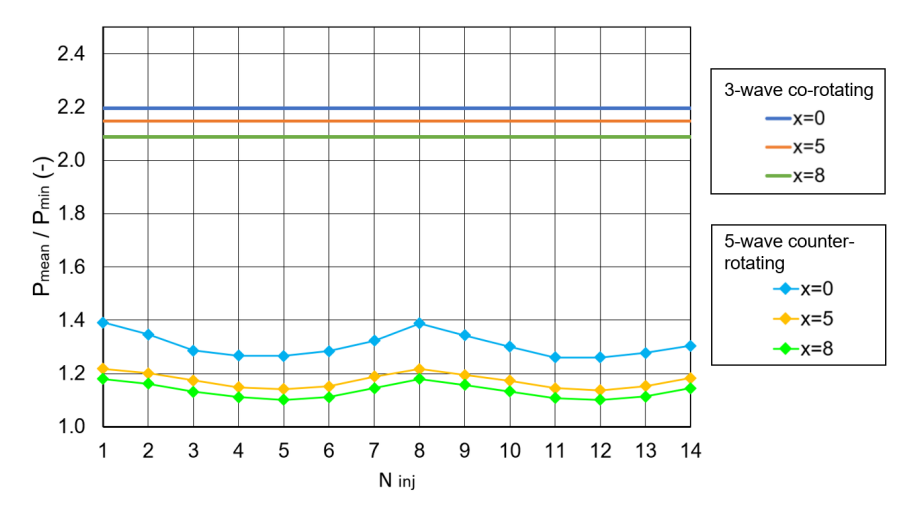


Fig 17. Normalized mean pressures at different distances from the injector (in mm): comparison of co-rotating vs counter-rotating regimes

This allows us to confirm that counter-rotating waves propagate in a degenerative mode, producing less pressure gain compared to co-rotating modes. Our interpretation is that the counter-rotating regime results from a non-homogeneity in the mixing or a temporary decay to deflagration, which might later transit back to a detonation via a pressure wave in the backward direction, as observed by [9, 8].

5. Conclusion

A sub-scale RDE combustor using gaseous H_2/O_2 has been studied and tested in cooperation between DLR and ONERA. Data on injection parameters and detonation characteristics (wave number, direction, and velocity) have been gathered at the Lampoldshausen Centre of DLR. Using the CEDRE code owned by ONERA, an LES approach is used for computations of the RDC with the injector. The unsteady effects of periodic detonations on injection and mixing, as well as an overview of the quality and main characteristics of the refilling process, are discussed. This article focuses on the experimental and numerical results for the 3-wave co-rotating and 5-wave counter-rotating cases, illustrating the alignment between both methods and offering insights into the mechanisms driving specific detonation regimes, with a focus on the fresh mixture formation and conditions in the refill region.

6. Acknowledgment

This project was provided with computing HPC and storage resources by GENCI at TGCC, thanks to the grant 2025-A0182B14179 on the supercomputer Joliot Curie's ROME partition.

References

[1] W. Armbruster, M. Börner, A. Bee, J. Martin, B. Knapp, S. General, J. Hardi, and E. Bard. Experimental investigation of a small-scale oxygen-hydrogen rotating detonation rocket combustor. In AIAA SCITECH 2024 Forum. AIAA, 2024.

- [2] E. Bach, C. O. Paschereit, P. Stathopoulos, and M. D. Bohon. An empirical model for stagnation pressure gain in rotating detonation combustors. *Proceedings of the Combustion Institute*, 38(3):3807–3814, 2021.
- [3] E. Bard, W. Armbruster, S. General, B. Knapp, A. Bee, M. Börner, K. Manassis, F. Strauss, J. Hardi, D. Davidenko, et al. Investigation on the influence of operation and injection conditions on the wave dynamics of gh2/go2 rotating detonation combustors. *Proceedings of the 35th ISTS & 14th NSAT*, 2025.
- [4] E. Bard, W. Armbruster, K. Rheindorf, A. Bee, M. Börner, S. General, J. S. Hardi, D. Davidenko, S. Boulal, and P. Vidal. Experimental study of a subscale rotating detonation chamber fed with gh2 / go2. 2024.
- [5] J. Bennewitz, B. Bigler, W. Hargus, S. Danczyk, and R. Smith. Characterization of detonation wave propagation in a rotating detonation rocket engine using direct high-speed imaging. In *The Review* of Scientific Instruments, 2018.
- [6] J. Bennewitz, B. Bigler, S. Schumaker, and W. J. Hargus. Automated image processing method to quantify rotating detonation wave behavior. In *The Review of Scientific Instruments*, page 90(6), 2019.
- [7] R. Bluemner, M. D. Bohon, C. O. Paschereit, and E. J. Gutmark. *Single and Counter-Rotating Wave Modes in an RDC*. 2018.
- [8] S. Boulal. *Comportements dynamiques de la détonation dans des compositions gazeuses non-uniformes*. PhD thesis, ISAE-ENSMA Ecole Nationale Supérieure de Mécanique et d'Aérotechique-Poitiers, 2017.
- [9] J. R. Burr and K. H. Yu. Detonation reignition within a rotating detonation engine. In *54th AIAA Aerospace Sciences Meeting*, page 1202, 2016.
- [10] F. A. Bykovskii, S. A. Zhdan, and E. F. Vedernikov. Continuous spin detonations. *Journal of Propulsion and Power*, 22:1204–1216, 2006.
- [11] P. A. Cocks, A. T. Holley, and B. A. Rankin. High fidelity simulations of a non-premixed rotating detonation engine. In *54th AIAA aerospace sciences meeting*, page 0125, 2016.
- [12] D. Davidenko, I. Gökalp, E. Dufour, and P. Magre. Numerical simulation of hydrogen supersonic combustion and validation of computational approach. In *12th AIAA international space planes and hypersonic systems and technologies*, page 7033. 2003.
- [13] D. Davidenko, I. Gökalp, and A. N. Kudryavtsev. Numerical simulation of the continuous rotating hydrogen-oxygen detonation with a detailed chemical mechanism. 2007.
- [14] S. Frolov, V. Aksenov, V. Ivanov, S. Medvedev, I. Shamshin, N. Yakovlev, and I. Kostenko. Rocket engine with continuous detonation combustion of the natural gas—oxygen propellant system. In *Doklady physical chemistry*, volume 478, pages 31–34. Springer, 2018.
- [15] T. Gaillard, D. Davidenko, and F. Dupoirieux. Numerical simulation of a rotating detonation with a realistic injector designed for separate supply of gaseous hydrogen and oxygen. *Acta Astronautica*, 141:64–78, 2017.
- [16] P. Hellard, T. Gaillard, and D. Davidenko. Evaluation of a computational strategy to model transitory injection in rotating detonation combustors. *Frontiers in Aerospace Engineering*, 2:1127671, 2023.
- [17] T. Kaemming, M. L. Fotia, J. Hoke, and F. Schauer. Thermodynamic modeling of a rotating detonation engine through a reduced-order approach. *Journal of Propulsion and Power*, 33(5):1170–1178, 2017
- [18] B. Le Naour, D. Davidenko, T. Gaillard, and P. Vidal. Rotating detonation combustors for propulsion: Some fundamental, numerical and experimental aspects. In I. Simone Salvadori, Polytechnic University of Turin, editor, *Front. Aerosp. Eng. volume* 2. Front. Aerosp. Eng. 2:1152429, 2023.
- [19] C. Le Touze, A. Murrone, and H. Guillard. Multislope muscl method for general unstructured meshes. *Journal of Computational Physics*, 284:389–418, 2015.
- [20] X.-Y. Liu, Y.-L. Chen, Z.-J. Xia, and J.-P. Wang. Numerical study of the reverse-rotating waves in rotating detonation engine with a hollow combustor. *Acta Astronautica*, 170:421–430, 2020.
- [21] A. Naples, J. Hoke, R. T. Battelle, M. Wagner, and F. R. Schauer. Rde implementation into an open-loop t63 gas turbine engine. In *55th AIAA aerospace sciences meeting*, page 1747, 2017.
- [22] P. Nassini et al. High-fidelity numerical investigations of a hydrogen rotating detonation combustor.

2022.

- [23] P. Pal, C. Xu, G. Kumar, S. A. Drennan, B. A. Rankin, and S. Som. Large-eddy simulations and mode analysis of ethylene/air combustion in a non-premixed rotating detonation engine. In *AIAA propulsion and energy 2020 forum*, page 3876, 2020.
- [24] S. Prakash, V. Raman, C. F. Lietz, W. A. Hargus Jr, and S. A. Schumaker. Numerical simulation of a methane-oxygen rotating detonation rocket engine. *Proceedings of the Combustion Institute*, 38(3):3777–3786, 2021.
- [25] A. Refloch, B. Courbet, A. Murrone, P. Villedieu, C. Laurent, P. Gilbank, J. Troyes, L. Tessé, G. Chaineray, J. Dargaud, E. Quémerais, and F. Vuillot. Cedre software. *AerospaceLab Journal*. 03 2011.
- [26] J. Sun, J. Zhou, S. Liu, and Z. Lin. Numerical investigation of a rotating detonation engine under premixed/non-premixed conditions. *Acta astronautica*, 152:630–638, 2018.
- [27] P. Wolanski. Detonation engines. Journal of KONES Powertrain and Transport, 18:515–521, 2011.